2019

Track structure simulations of proximity functions in liquid water using the Geant4-DNA toolkit

Sebastien Incerti
Universite de Bordeaux, incerti@cenbg.in2p3.fr

Ioanna Kyriakou
University of Ioannina

M Bordage
University of Toulouse

Susanna Guatelli
University of Wollongong, susanna@uow.edu.au

Vladimir N. Ivanchenko
Tomsk State University

See next page for additional authors

Recommended Citation

Track structure simulations of proximity functions in liquid water using the Geant4-DNA toolkit

Abstract

The mechanistic Monte Carlo modeling of biological effects of ionising radiation at sub-cellular and DNA scale requires the accurate simulation of track structures in the biological medium, commonly approximated as liquid water. The formalism of microdosimetry allows one to describe quantitatively the spatial distribution of energy deposition in the irradiated medium, which is known to relate to the deleterious effects in the irradiated cellular targets. The Geant4-DNA extension of the Geant4 open-source and general-purpose Monte Carlo simulation toolkit has been recently evaluated for the simulation of microdosimetry spectra, allowing, in particular, the calculation of lineal energy distributions. In this work, we extend the microdosimetric functionalities of Geant4-DNA by the development of a new Geant4-DNA example dedicated to the simulation of differential proximity functions. Simulation results are presented for the proximity function of electrons, protons, and alpha particles over a wide energy range using the different physical models of electron interactions available in Geant4-DNA. The influence of sub-excitation processes and electron tracking cut is discussed. Results are compared to literature data when available. As an example, a simple calculation of the relative biological effectiveness (RBE) in the context of the Theory of Dual Radiation Action using the present proximity functions yields up to a factor of 2 variation of the electron RBE in the energy range from 100 eV to 100 keV.

Disciplines

Engineering | Science and Technology Studies

Publication Details

Authors

Sebastien Incerti, Ioanna Kyriakou, M Bordage, Susanna Guatelli, Vladimir N. Ivanchenko, and Dimitris Emfietzoglou

Track structure simulations of proximity functions in liquid water using the Geant4-DNA toolkit

S. Incerti (iD), I. Kyriakou, M. C. Bordage (iD), S. Guatelli, V. Ivanchenko (iD), and D. Emfietzoglou

View Online   Export Citation   CrossMark

ARTICLES YOU MAY BE INTERESTED IN

Track structure simulations of proximity functions in liquid water using the Geant4-DNA toolkit

S. Incerti,[1,2,a)] I. Kyriakou,[3] M. C. Bordage,[4,5] S. Guatelli,[6,7] V. Ivanchenko,[8,9] and D. Emfietzoglou[3,a)]

AFFILIATIONS

[1]University of Bordeaux, CENBG, 33170 Gradignan, France
[2]CNRS, IN2P3, CENBG, 33170 Gradignan, France
[3]Medical Physics Laboratory, University of Ioannina Medical School, 45110 Ioannina, Greece
[4]Université Toulouse III-Paul Sabatier, UMR1037 CRCT, 31037 Toulouse, France
[5]Inserm, UMR1037 CRCT, 31037 Toulouse, France
[6]Centre for Medical Radiation Physics, University of Wollongong, Wollongong, NSW 2522, Australia
[7]Illawarra Health and Medical Research Institute, University of Wollongong, Wollongong, NSW 2522, Australia
[8]Geant4 Associates International Ltd., Hebden Bridge, United Kingdom
[9]Tomsk State University, Tomsk, Russia

[a)]Authors to whom correspondence should be addressed: incerti@cenbg.in2p3.fr and demfietz@uoi.gr

ABSTRACT

The mechanistic Monte Carlo modeling of biological effects of ionising radiation at sub-cellular and DNA scale requires the accurate simulation of track structures in the biological medium, commonly approximated as liquid water. The formalism of microdosimetry allows one to describe quantitatively the spatial distribution of energy deposition in the irradiated medium, which is known to relate to the deleterious effects in the irradiated cellular targets. The Geant4-DNA extension of the Geant4 open-source and general-purpose Monte Carlo simulation toolkit has been recently evaluated for the simulation of microdosimetry spectra, allowing, in particular, the calculation of lineal energy distributions. In this work, we extend the microdosimetric functionalities of Geant4-DNA by the development of a new Geant4-DNA example dedicated to the simulation of differential proximity functions. Simulation results are presented for the proximity function of electrons, protons, and alpha particles over a wide energy range using the different physical models of electron interactions available in Geant4-DNA. The influence of sub-excitation processes and electron tracking cut is discussed. Results are compared to literature data when available. As an example, a simple calculation of the relative biological effectiveness (RBE) in the context of the Theory of Dual Radiation Action using the present proximity functions yields up to a factor of 2 variation of the electron RBE in the energy range from 100 eV to 100 keV.

I. INTRODUCTION

Monte Carlo codes for track structure (TS) simulations in liquid water are recognized today as the most adapted theoretical tools for the mechanistic investigation of biological effects of ionising radiation at the sub-cellular and DNA scale.[1–4] They not only provide a way to compute physical quantities where experimental data are often lacking[5] but also ensure better accuracy than "condensed-history" Monte Carlo codes[6,7] at low electron energies (below a few keV) and small volumes (micro- and nanometer scale).[8–13] Several Monte Carlo TS (MCTS) codes have been developed for radiation biophysics applications, with notable examples being the NOREC,[14] PARTRAC,[15] and KURBUC[16] codes, among others.[17] The Geant4-DNA extension[5,18–20] of the open-source and general-purpose Geant4 Monte Carlo simulation toolkit[21–23] provides in full open access a variety of discrete physics models for TS simulations in the biological medium.

Liquid water is the most abundant constituent of human body and cells; therefore, it is traditionally considered as a surrogate to the biological medium.[3,17] Thus, the calculations presented in this work are all performed in liquid water. In an effort to describe

more accurately the biological medium, some MCTS codes also include models describing the physical interactions of ionising radiation in more realistic biological targets such as DNA components. For example, the CPA100,[24] RETRACKS,[25] and Geant4-DNA[26] codes, among others, propose cross sections for the simulation of step-by-step interactions of electrons in adenine, thymine, guanine, cytosine, and sugar-phosphate components of DNA in the gas phase. However, a careful validation of such models against experimental data in the condensed-phase of the biological medium is still missing. In addition, a lack of international recommendations on fundamental quantities related to radiation transport (e.g., range and stopping power from ICRU) in such biological media (other than liquid water), especially at very low energies (sub-keV range), make their usage still very uncertain for TS simulations. For all the above reasons, state-of-the-art MCTS biophysical codes, like PARTRAC and KURBUC, are still using liquid water as an approximation to the biological medium and have been particularly successful in simulating biological damage induced by ionising radiation.[3,27] For these reasons, all simulations presented in this work use liquid water as an approximation for the biological medium.

The continuous development of discrete physics models for TS simulations[28–35] is of outmost importance for improving the description of the energy deposition pattern in the irradiated medium at the nano- and micrometer scales using MCTS codes. Such energy depositions are responsible for inducing direct and indirect (via water radiolysis) early damage to DNA.[36,37] In order to evaluate the accuracy of TS simulations and facilitate their use in a wide range of applications, Geant4-DNA provides a set of 11 ready-to-use example applications[20] (so-called "extended examples"), which can calculate both fundamental quantities (e.g., range, stopping power, mean free path) and dosimetry-related quantities (e.g., lineal energy, specific energy, dose-point-kernel, S-value). Beyond their pedagogical role, these examples also serve as benchmarks to compare the Geant4-DNA accuracy for TS simulations versus international recommendations, other codes and experimental data, when they are available.

The microdosimetry formalism[38,39] allows one to quantitatively describe energy deposition in irradiated sub-cellular volumes.[40] We recently investigated the performance of Geant4-DNA for the simulation of frequency-mean and dose-mean lineal energies,[8] underlining, in particular, the necessity to adopt the TS approach[9] when the target dimension is much smaller than the ionising particle track length. Geant4-DNA users can extract distributions of lineal energies (and also specific energies) using the dedicated "microyz" extended example.

Another fundamental description of the energy deposition patterns is obtained through the differential proximity functions of radiation tracks.[38] These functions are defined as the mean energy deposited to a spherical shell of given radius and thickness centered at a randomly chosen energy-transfer point in the shower of tracks induced by a primary particle and all its secondaries. They are thus particularly useful for the study of interaction of pairs of sublesions which are implicated in various biophysical models of radiation action[41] (e.g., in the context of the Theory of Dual Radiation Action, TDRA[42]). The simulation of proximity functions requires an accurate modelling of step-by-step physical interactions of particles, with a spatial resolution compatible with biological target

dimensions (sub-micrometer scale for cells) and down to very low energies (eV scale). This is particularly important for an accurate modeling of secondary electrons tracks, which are the main source of damage in radiobiology.[3] Such an accuracy requires notably a fine description of particle physical interactions (e.g., ionisation, excitation, elastic scattering, etc.), starting from cross sections and including a complete picture of the final state of the interaction (e.g., energy loss, scattering of the incident particle, ejection of secondary particles if any, etc.). Although numerous research groups are proposing different theoretical and/or semi-empirical models to describe such interactions in liquid water, a unique picture describing these interactions in liquid water over a broad energy range is still missing, especially at very low energies (below about 1 keV), where it remains a challenge to perform measurements in the liquid phase of water.[34] Therefore, published works describing the simulation of proximity functions usually adopt different models describing these physical interactions. This work focuses on the simulation of proximity functions using the models available in the Geant4-DNA very low energy extension of Geant4.

Proximity functions of radiation tracks have been studied by several authors, particularly for electrons, since secondary electrons are mainly responsible for radiation damage. Almost four decades ago, Chmelevsky et al.[43] simulated proximity functions for electrons in water up to 10 keV using the Monte Carlo code developed by Terrissol[24] and illustrated their usage for the extraction of the dose-average lineal energies in spheres of water. Brenner and Zaider[44] calculated microdosimetric quantities including proximity functions for electrons and protons in vapor water using their Monte Carlo code. Leuthold and Burger[45] presented Monte Carlo simulations of proximity functions for protons in vapor water from 0.2 to 15 MeV also using their own Monte Carlo code. Dayashankar and Prasad[46] presented fast semi-analytical calculations of proximity functions for electrons from 10 eV up to 10 keV in vapor water and verified their results using Monte Carlo simulations. Taschereau et al.[47] calculated electron proximity functions using the so-called "Livermore" set of condensed-history low-energy electromagnetic models of Geant4 in the 1–35 keV range, in order to extract dose-average specific energy from single-event distributions for a given cell line (V79) and calculate RBE. Chen and Kellerer[48] provided a comprehensive database of calculated proximity functions for electrons from 100 eV up to 10 MeV using an updated version of the Monte Carlo code of electrons in vapor water by Zaider et al.[49] Dabli[50] presented calculations of proximity functions for the first set of models that was provided in Geant4-DNA (version 9.2),[5] underlining the better accuracy obtained with Geant4-DNA compared to other Geant4 electromagnetic models, as we also reported for the simulation of microdosimetric quantities.[8,9] Finally, and more recently, Emfietzoglou et al.[51] calculated electron proximity functions in the 50 eV–5 keV energy range, using an in-house MC code based on the Emfietzoglou-Cucinotta-Nikjoo (ECN) model[52] of the dielectric function of liquid water and compared their results to the dielectric model of the Oak Ridge National Lab (ORNL) noting sizeable differences between models up to several nanometers. Although these works clearly underline theoretical progress for the development of more accurate Monte Carlo simulations of microdosimetry spectra and proximity functions, they do not provide an easy access to such TS simulations.

In this work, we describe a new Geant4-DNA application dedicated to the simulation of differential proximity functions in liquid water, for various radiation qualities. This application will become a new Geant4 example which will be released publicly. Section II briefly describes the Geant4-DNA physics processes and models available for TS simulations in liquid water. We then present the calculation of proximity functions and introduce the new "microprox" extended example. In Sec. III, we calculate proximity functions for electrons, protons, and alpha particles over a wide energy range using the three sets of physics constructors available in Geant4-DNA. Results are compared to other Monte Carlo simulation results from the literature and are discussed. A simple application of the present results to the theoretical calculation of RBE in the context of the TDRA is also presented.

II. MATERIAL AND METHODS

A. Geant4-DNA processes and models

Geant4-DNA can simulate TS of electrons, protons, neutral hydrogen, alpha particles and their charged states, and a few ion species (dominant in the cosmic spectrum) in liquid water. We note that TS simulations in the DNA material (instead of liquid water) are out of the scope of this work. Electron interactions on water molecules include inelastic interactions (that is, ionisation, electronic excitation, and vibrational excitation), elastic scattering, and molecular attachment. The interactions of protons, neutral hydrogen atoms, alpha particles, and their charged states include inelastic interactions (ionisation and electronic excitation), elastic scattering, and capture or loss of electrons. Regarding ions, only the ionisation process is currently available in Geant4-DNA, preventing for accurate step-by-step simulations at very low energy where other processes (e.g. electronic excitation and charge exchange processes) cannot be neglected. All these particles can be tracked down to a cut off value, below which their kinetic energy is deposited locally into the irradiated medium. Geant4-DNA proposes three recommended alternative physics constructors,[20] which gather the list of particles and physical interactions they can undergo. These constructors, called "G4EmDNAPhysics_option2," "G4EmDNAPhysics_option4," and "G4EmDNAPhysics_option6," are denoted as "option 2," "option 4," and "option 6," respectively, in the following text. These three constructors differ only by the models they use to calculate electron interactions. These electron models have been calculated using different approaches as it has been already described in previous publications.[19] In short, the "option 2" constructor contains the first set of models that was initially proposed in Geant4-DNA for the simulation of electron tracks in liquid water.[5,20] The inelastic cross sections for the individual ionisation and excitation channels of the weakly bound electrons of liquid water are calculated in the first Born approximation (FBA) from the complex dielectric response function of liquid water proposed by Emfietzoglou.[53] A kinematic Coulomb-field correction and Mott-like exchange-correction terms are used below a few hundred eV to improve the FBA calculations. Cross sections for electron-impact ionisation of the K-shell of the oxygen atom are calculated analytically from the Binary-Encounter-Approximation-with-Exchange (BEAX) model. Elastic cross sections are based on partial wave calculations. The "option 4" constructor provides a

more accurate set of ionisation and excitation cross sections based on an improved implementation of the complex dielectric response function of liquid water.[54] The application of Coulomb and Mott corrections has also been revised and implemented in a more consistent manner.[54] Resulting excitations are strongly enhanced relative to ionisations. This leads to higher mean energies required for the creation of an ion pair in liquid water, smaller penetration distances, and less diffused dose point kernels at sub-keV electron energies.[55] Elastic scattering is based on the screened Rutherford model with empirical parameters based on data in the vapor phase of water. Finally, the "option 6" constructor is a porting of the CPA100 TS code (which is not developed anymore) to Geant4. Cross sections for electronic excitations are calculated in the FBA using the complex dielectric response function developed by Dingfelder and co-workers, ionisation cross sections are calculated from the Binary-Encounter-Bethe (BEB) model, and elastic scattering cross sections are based on partial wave calculations using the independent atom approximation.[56] An overview of the electron models (including the tracking cut) is presented in Table I. On the contrary, the models used to simulate the interactions of protons, neutral hydrogen atoms, alpha particles and their charged states, and ions are identical in all three constructors.[19] Finally, atomic deexcitation (emission of Auger electrons and fluorescence photons) is simulated using the EADL database as discussed elsewhere.[57]

B. Computation of proximity functions

The computation of proximity functions is performed by simulating TS of incident particles (electrons, protons, and alpha particles) in liquid water using Geant4-DNA processes. Geant4-DNA simulates all physical interactions in a step-by-step (also called "discrete") mode: the interactions of the primary particle and all secondaries are simulated until all particles reach a low energy tracking cut. For electrons, this cut is set to 7.4 eV, 10 eV, or 11 eV, in "option 2," "option 4," and "option 6" physics constructors, respectively, and corresponds to the low energy limit of applicability of the physics models of the constructors. Refer to Table I for the detail of models and their energy range of applicability. Protons and alpha particles, including their charged states, are tracked down to 100 eV and 1 keV, respectively. For each incident particle simulated, an energy deposition ε_i is selected among all energy depositions occurring in the entire track. Spherical shells of varying radius x are then centered on the selected energy deposition (ε_i) and the energy depositions (ε_k) of the entire track which are located within this shell are summed up. The same procedure is repeated for all other energy depositions in the entire track. This is illustrated in Fig. 1. The differential proximity function,[48] $t(x)$, is then extracted by calculating the following ratio:

$$t(x)dx = \sum_{i,k} \varepsilon_i \varepsilon_k / \sum_i \varepsilon_i, \qquad (1)$$

where dx is the shell thickness. In the above formula, the summation in the numerator runs over all energy depositions of the track structure (ε_i) and on energy depositions (ε_k) located within the spherical shell only. The summation in the denominator runs on all energy depositions of the track structure. Each summation over

TABLE I. List of Geant4-DNA sets of electron cross section models available in Geant4-DNA physics constructors. Energy ranges of applicability and default tracking cuts are indicated as well. The models are described in more details in the given references.

	Geant4-DNA physics constructor[20]		
	G4EmDNAPhysics_option2 ("option 2")[5]	G4EmDNAPhysics_option4 ("option 4")[54,55]	G4EmDNAPhysics_option6 ("option 6")[19,56]
Energy range of applicability	7.4 eV–1 MeV	10 eV–10 keV	11 eV–256 keV
Ionisation	Emfietzoglou optical-data model of the dielectric function with Born corrections (11 eV–1 MeV)	Kyriakou-Emfietzoglou optical-data model dielectric function with Born corrections (10 eV–10 keV)	Relativistic Binary Encounter Bethe model (11 eV–256 keV)
Excitation	Same as ionisation (9 eV–1 MeV)	Same as ionisation (8 eV–10 keV)	Differential oscillator strength from the Dingfelder model of the dielectric response function (11 eV–256 keV)
Elastic	Partial-wave analysis (7.4 eV–1 MeV)	Rutherford formula with screening term by Uehara et al.[69] (9 eV–10 keV)	Independent Atom Method (11 eV–256 keV)
Vibrational excitation	Sanche data (2 eV–100 eV)	n/a	n/a
Molecular attachment	Melton data (4 eV–13 eV)	n/a	n/a
Tracking cut	7.4 eV	10 eV	11 eV
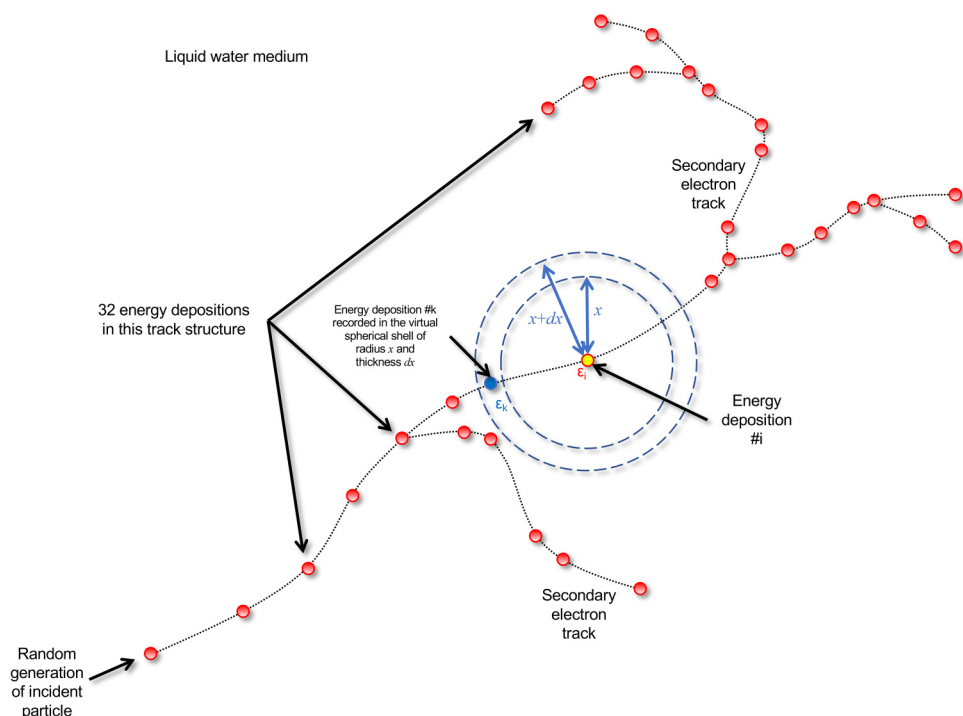
FIG. 1. Principle of calculation of differential proximity functions $t(x)$ for the track structure of a single incident particle. The track structure illustrated in this figure contains a total of 32 energy depositions (each being represented by a red disk) induced by the incident particle and its secondaries. For each energy deposition (e.g., for energy deposition ε_i marked as a yellow disk) among these 32 depositions, the total energy absorbed in spherical shells of varying radius x and thickness dx (represented by the two blue dashed circles, where the energy deposition ε_k—in blue—is recorded) centered on this energy deposition is recorded. The same procedure is repeated over all remaining 31 energy depositions weighted by their energy value ε_i divided by the total energy deposited in the track, in order to calculate $t(x)dx$ from formula (1). The average value of $t(x)dx$ is obtained by simulating a large number of independent tracks.

the energy depositions (ε_k) located within the spherical shell is thus weighted by the ratio of ε_i to the total energy deposition in the medium. This calculation is repeated over a large number of independent incident particles, up to 10^6 electrons for the lowest incident energies, in order to extract mean values.

Calculations presented in this work investigate the influence of physics models on proximity functions through the three recommended "option 2," "option 4," and "option 6" physics constructors available in Geant4-DNA.[20] This notably includes the effect of electron sub-excitation processes (vibrational excitation and molecular attachment which are simulated in the "option 2" constructor only). The influence of the tracking cut is also investigated.

C. The "microprox" Geant4 extended example

We recently published a detailed report describing all Geant4-DNA examples available in Geant4 for TS simulations in liquid water.[20] The new "microprox" extended example will be delivered in Geant4 after publication of this work. This new Geant4-DNA example explains to users how to simulate differential proximity functions for different radiation qualities. The user has the possibility to select in the application a range of values for the spherical shell radii (specifying minimum value, maximum value, and number of bins). The values of the radii are calculated with equal spacing in a logarithmic scale so that they can cover a large range of values, as usually found in the literature (several orders of magnitude). In addition, the tracking cut of particles in the simulation can be changed in the application. Mean differential proximity functions $t(x)$ for spherical shells of radius x in the specified range of values are calculated and expressed in (eV/nm) using the provided ROOT[58] macro file ("plot.C"). In the presented plots, the function values are shown at each radial value x (of width dx) displayed in the logarithmic scale. Each curve contains 100 values except for 1 MeV incident electrons, and for protons and alpha particles where 40 values are computed, for faster simulations. This example is fully compatible with the multithreading[23] feature of Geant4, allowing a significant speedup of simulations on recent multi-core computers. Geant4 users interested in such simulations may download our free Geant4 virtual machine (available from http://geant4.in2p3.fr) for the VMware™ or VirtualBox™ environments, which emulates a CentOS Linux™ machine where Geant4 is already installed and ready-to-use, including all Geant4-DNA examples.

III. RESULTS AND DISCUSSION

A. Electron simulations

Differential proximity functions have been calculated for incident monoenergetic electrons in the 50 eV to 1 MeV range. We first describe the verification of the simulations. Then, we present the results obtained for the three different physics constructors, as well as the influence of sub-excitation processes (for the "option 2" constructor only). Simulations are compared to data from the literature and the influence of the tracking cut is discussed. The reader should keep in mind that a full (and direct) validation of such simulation remains currently impossible since experimental data on proximity functions in liquid water do not exist.

1. Verification of simulations

A first verification of simulations can be undertaken knowing that the integral of the differential proximity function is equal to the total energy absorbed in the medium

$$\int_0^\infty t(x)dx = E_{tot}, \quad (2)$$

where in the case of an infinite medium, $E_{tot} = E_{inc}$, i.e., the total energy absorbed equals the incident kinetic energy of the electron track. For example, for 100 eV incident electrons using the "option 2" physics constructor and integrating over 10^3 x-bins up to 100 nm, Eq. (2) is exactly verified. For 1 keV electrons, integrating up to 1 μm for the same number of bins, it is verified at the 10^{-3}% level.

As an additional verification, the dose-mean lineal energy y_D in a spherical scoring sphere of diameter d can be computed analytically as[59]

$$y_D = \frac{3}{2d} \int_0^d \left[1 - \frac{3x}{2d} + \frac{x^3}{2d^3} \right] t(x)dx, \quad (3)$$

[note that formula (7) of Ref. 59 has a wrong $3d/2$ factor, which should read instead $3/2d$]. We recently published a study on the simulation with Geant4-DNA of microdosimetry quantities[8] including dose-mean lineal energy in liquid water (see Fig. 9 of Ref. 8), using the dedicated "microyz" Geant4-DNA example. In order to verify the self-consistency of the proximity functions obtained from simulations of this work, we compared y_D values calculated using Eq. (3) and values shown in Ref. 8, assuming identical simulation settings (same physics constructor, a tracking cut of 11 eV and no activation of sub-excitation processes). Results are presented in Table II and show a good agreement at the few percent level, especially for the largest diameters (10 nm and 30 nm).

2. Influence of physics constructor

Figure 2 shows the differential proximity functions obtained for 50 eV, 100 eV, 1 keV, 10 keV, 100 keV, and 1 MeV monoenergetic electrons using the "option 2," "option 4," and "option 6" constructors with the default tracking cut (7.4 eV, 10 eV, and 11 eV, respectively). The maximum energy shown for "option 4" is 10 keV, and it is 100 keV for "option 6" because of the maximum energy limit of applicability of the constructor (see Table I). Globally, for a given incident energy, all plots show similar profiles on the 0.1 nm–100 nm range. For a given constructor, the maximum of the curves increases slightly with an incident energy from 50 eV up to 1 keV (shifting from 1 nm to a few nm), then decreases again, moving back to lower radius values. As it is expected, the extension of the proximity function increases with the electron energy due to the larger distance travelled by the incident particle. It is important to notice that the proximity function changes significantly at low energies (i.e., the 50, 100, 1000 eV curves are very different), whereas it remains less sensitive to the incident energy at higher energies (i.e., the 10, 100, 1000 keV curves are very similar). This clearly illustrates that the "quality" of

TABLE II. Comparison of y_D values for incident monoenergetic electrons calculated either analytically from Eq. (3) or obtained using the dedicated "microyz" Geant4-DNA example (results from Fig. 9 of Ref. 8).

Energy of electron tracks	Diameter of scoring sphere (nm)		
	2	10	30
100 eV	y_D = 24.2 eV/nm from Eq. (3)	10.6 eV/nm from Eq. (3)	4.5 eV/nm from Eq. (3)
	23.4 eV/nm from Ref. 8	10.5 eV/nm from Ref. 8	4.4 eV/nm from Ref. 8
1 keV	27.5 eV/nm from Eq. (3)	23.5 eV/nm from Eq. (3)	20.6 eV/nm from Eq. (3)
	26.6 eV/nm from Ref. 8	23.2 eV/nm from Ref. 8	20.5 eV/nm from Ref. 8

low-energy electrons changes rapidly with energy, while it remains rather constant above about 10 keV. The implication of the changing shape of the proximity function with electron energy will be discussed below in the context of biophysical modeling. At 50 eV, "option 2" maximum is located close to 1 nm and reaches about 9 eV/nm. In the case of "option 4," the maximum is also at 1 nm reaching 12 eV/nm. For "option 6," the maximum is located at smaller radius than for the two other constructors, that is, at about 0.4 nm and reaching about 19 eV/nm. At 1 keV, the maximum for "option 2" is reached near 4 nm and close to 45 eV/nm; "option 4" maximum is located near 3 nm and reaches 46 eV/nm, and "option 6" maximum is at 1.8 nm and reaches about 52 eV/nm. These observations are consistent with the fact that the sum of inelastic cross sections of "option 6" (responsible for the energy losses) are larger (see Fig. 4 of Ref. 19) than for the two other constructors on the entire energy range covered by these constructors.

They also show that the "option 6" constructor, while behaving similarly as the two other constructors, predicts larger proximity functions.

### 3. Influence of sub-excitation processes

The "option 2" constructor includes sub-excitation processes, which are applied to low energy electrons. These two processes, vibrational excitation (applicable below 100 eV) and molecular attachment (applicable below 13 eV), are needed for the simulation of the physico-chemical stage of water radiolysis down to thermalization.[60] These processes are responsible for additional energy losses (vibrational excitation) or for the disappearance of electrons which attach to surrounding water molecules. These processes have not been included so far in the two other constructors since their energy range of applicability is limited and they are not yet used for the simulation of water radiolysis.[19] The influence of these two processes is shown in Fig. 3. The full lines represent "option 2" differential proximity functions considering these sub-excitation processes, while the dashed lines are obtained when these two processes are deactivated. In these simulations, a tracking cut of 9 eV has been used, equal to the low energy applicability limit of the electronic excitation (9 eV) process of "option 2." Both configurations lead to similar results, noting however that before and at the maxima, proximity functions with sub-excitation processes are slightly larger than the case when these processes are not considered. On the opposite, beyond the maxima and at large radii, they become slightly smaller. For example, at 50 eV, the maximum with sub-excitation processes reaches 9.1 eV/nm, while it reaches

8.2 eV/nm without sub-excitation processes. At 1 keV, the maximum with sub-excitation processes reaches 44.8 eV/nm and 41.2 eV/nm without them. This is a consequence of the additional energy deposition induced by vibrational excitation which tends to increase energy depositions at smaller distances.

4. Comparison with literature data

In Figs. 4 and 5, we compare the present simulation results with available data in the literature. For a meaningful comparison, we have carried out additional Geant4-DNA simulations of proximity functions using identical tracking cuts with those used in the other studies. In Fig. 4, we compare Geant4-DNA simulations obtained with the three constructors to the simulations of differential proximity functions in liquid water performed by Chen and Kellerer[48] in vapor water, at five incident energies: 100 eV, 1 keV, 10 keV, 100 keV, and 1 MeV. The data of Chen and Kellerer have been digitized from the original publication. For these simulations, a tracking cut of 12.6 eV has been selected identical to the value used by Chen and Kellerer. In the case of 1 keV simulations, we also added to the figure the upper and lower limits (represented as black stars) of simulations performed by Brenner and Zaider, also performed in the vapor phase of water. It was not possible to clearly digitize all their results for the 5 overlapping curves shown in Fig. 3 of their work,[44] especially at large radii. For completeness, we also included the data of Dayashankar and Prasad[46] for vapor. These data were obtained for a much lower tracking cut value of 4.5 eV, which is much smaller than the low energy limit applicability of Geant4-DNA "option 2" physics constructor of 7.4 eV.

Globally, the shapes of all profiles are similar but there are significant differences in the distribution, especially at small distances (<10 nm). Obviously, since the three constructors and literature data use different models for the description of physical interactions of electrons in water, such differences are expected, especially at a very low energy. As an illustration, the reader is invited to consult Figs. 1–4 of Bernal et al.[19] illustrating the differences between cross section models for electrons in Geant4-DNA physics constructors. For example, "option 2" and "option 4" proximity function profiles are quite close on the entire energy range, since the corresponding cross sections are also close.[19] On the contrary, as already observed in Fig. 2, proximity functions obtained with "option 6" are clearly larger from those of "option 2" and "option 4." This is because both "option 6" and the physics models of the Monte Carlo code used by Chen and Kellerer are, to a large extent, atomic models. So, the effect of screening of the condensed-phase,
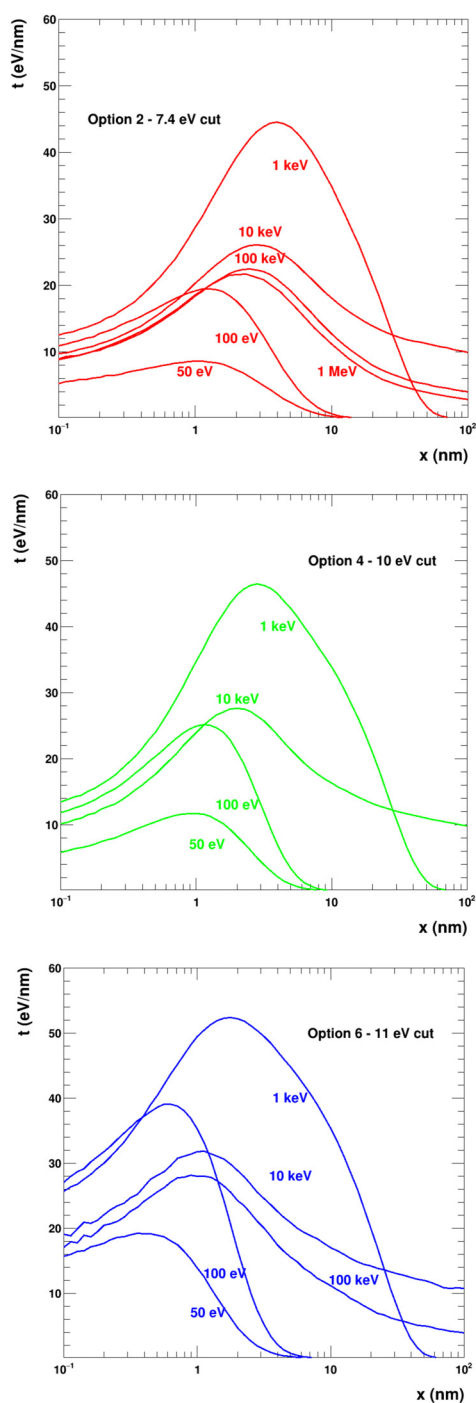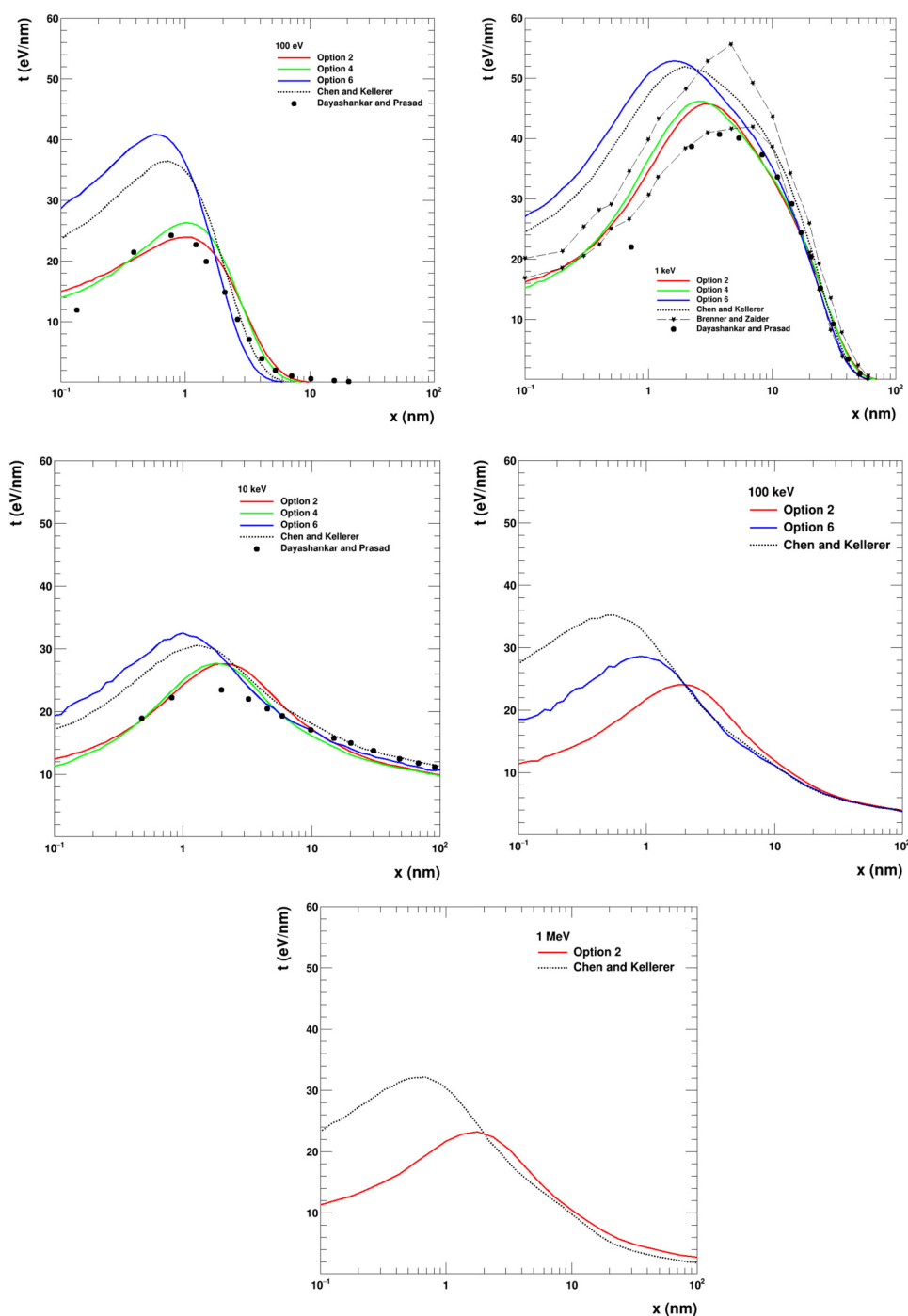
FIG. 2. (Differential) proximity function $t(x)$ as a function of radius x for monoenergetic electrons of 50 eV, 100 eV, 1 keV, 10 keV, 100 keV, and 1 MeV obtained with the three Geant4-DNA physics constructors, "option 2" (top plot, red curves), "option 4" (middle plot, green curves), and "option 6" (bottom plot, blue curves). The default tracking cut proposed by these constructors has been used: 7.4 eV for "option 2," 10 eV for "option 4," and 11 eV for "option 6."

which underlines both "option 2" and "option 4" (leading to lower inelastic cross sections), is disregarded. Regarding the proximity function calculations of Brenner and Zaider at 1 keV, they seem to be in reasonable agreement with "option 2" and "option 4" and less so with "option 6." Finally, the data of Dayashankar and Prasad[46] appear lower than Geant4-DNA "option 2" and "option 4" simulation results. They used a very low tracking cut (4.5 eV) compared to the 7.4 eV cut of Geant4-DNA "option 2." These lower proximity functions are a direct consequence of the lowering of the tracking cut, as we discuss further in Sec. III A 5.

In Fig. 5, we compare Geant4-DNA simulations to the recent results of Emfietzoglou et al.[51] at three incident energies: 50 eV, 100 eV, and 1 keV. In these simulations, the tracking cut was set to 1 Ry (13.606 eV) which was the value also used by Emfietzoglou et al.[51] Note that the data of Ref. 51 are multiplied by 2 due to an error in the shell thickness dx assumed 1 nm instead of 0.5 nm. The proximity functions of Emfietzoglou et al.[51] are overall closer to those obtained with "option 2" and "option 4." Electron transport in Emfietzoglou et al.[51] is also based on a similar parameterization of the dielectric function resulting in inelastic cross sections of comparable magnitude to "option 2" and "option 4." The observed differences can be attributed to the different dispersion relations adopted in the dielectric function of Ref. 51, which leads to somewhat larger mean free paths and a shift of the proximity function to larger distances compared to "option 2" and "option 4."
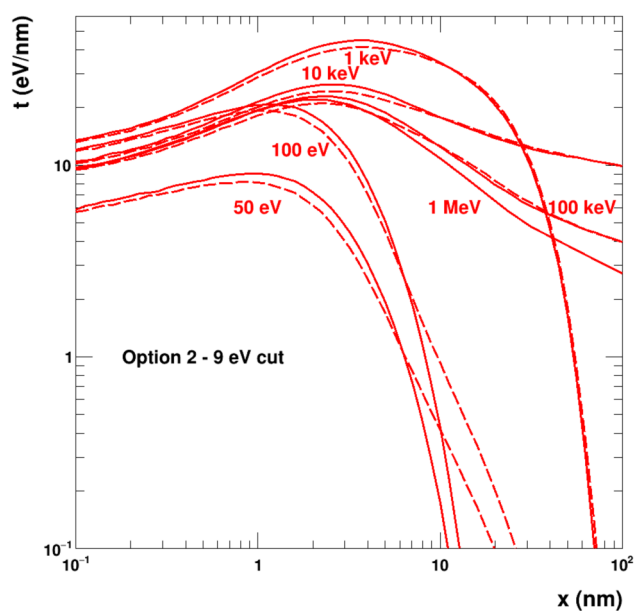
FIG. 3. (Differential) proximity function $t(x)$ as a function of radius x for monoenergetic electrons of 50 eV, 100 eV, 1 keV, 10 keV, 100 keV, and 1 MeV obtained with the "option 2" Geant4-DNA physics constructor. In these simulations, sub-excitation processes (vibrational excitation and molecular attachment) have been activated (full curves) or de-activated (dashed curves). A tracking cut of 9 eV has been applied to all simulations.
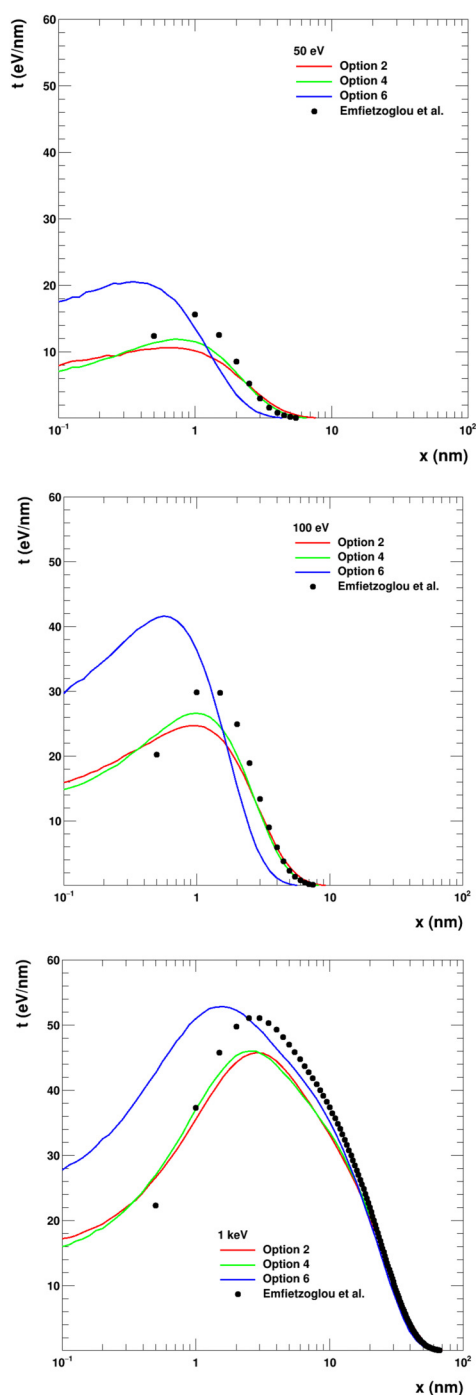
FIG. 4. (Differential) proximity functions $t(x)$ as a function of radius x for monoenergetic electrons with incident energies of 100 eV, 1 keV, 10 keV, 100 keV, and 1 MeV. For the comparison with the simulations of Chen and Kellerer[48] (black dotted line), a 12.6 eV tracking cut has been applied to all Geant4-DNA simulations. These simulations were performed using the three physics constructors "option 2" (red line), "option 4" (green line), and "option 6" (blue line). In the case of 1 keV electrons, upper and lower limits of proximity functions calculated by Brenner and Zaider[44] for the vapor phase are qualitatively shown by the black stars and the dashed lines. Finally, and for completeness, we also added the data of Dayashankar and Prasad[46] for vapor and for a 4.5 eV tracking cut (black disks).
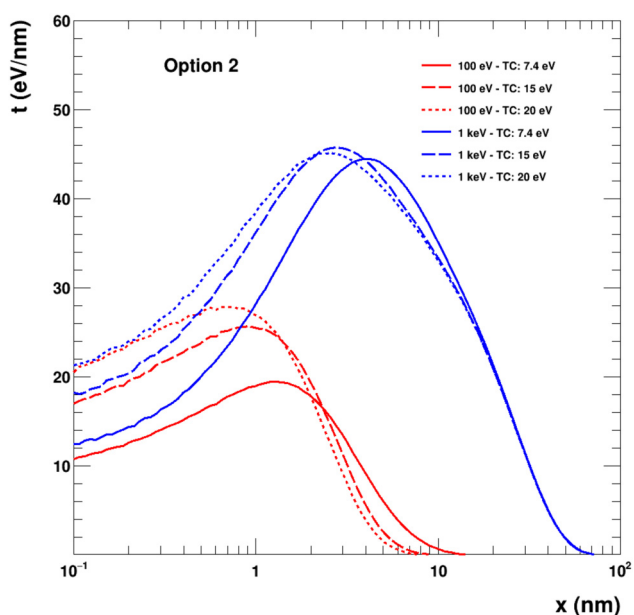
5. Influence of tracking cut

An important parameter that influences the simulation of proximity functions is the tracking cut below which the tracking of particles is stopped and their remaining kinetic energy is deposited locally. All MCTS codes have their own tracking cut, usually taken as the first electronic excitation level of liquid water (commonly taken to be in the range of 7–10 eV). The usage of different tracking cuts leads to different trajectory lengths for both the primary and secondary particles, which necessarily affect the pattern of energy deposition. In Fig. 6, we present the influence of the tracking cut

FIG. 6. (Differential) proximity functions $t(x)$ as a function of radius x for monoenergetic electrons with incident energies of 100 eV (red curves) and 1 keV (blue curves) obtained using the "option 2" physics constructor with three different tracking cuts (TCs): 7.4 eV (full line), 15 eV (long-dashed line), and 20 eV (short-dashed line).

FIG. 5. (Differential) proximity functions $t(x)$ as a function of radius x for monoenergetic electrons with incident energies of 50 eV, 100 eV, and 1 keV. For the comparison with the simulations of Emfietzoglou et al.[51] (black disks), a 13.606 eV tracking cut has been applied to all Geant4-DNA simulations. These simulations were performed using the three physics constructors "option 2" (red line), "option 4" (green line), and "option 6" (blue line).

on proximity functions. In this figure, the "option 2" constructors have been used to extract proximity functions at two incident energies, 100 eV and 1 keV, and for three tracking cuts: 7.4 eV (which is the default tracking cut of "option 2"), 15 eV, and 20 eV. Clearly, for both incident energies, we observe that lowering the tracking cut leads to a shift of the proximity function towards larger distances. This is expected since lowering the tracking cut results in a larger number of low energy secondary electron tracks (or trackends) which spread energy depositions in the 3D-space, thus depopulating regions with small radii around each energy deposition ε_i [see Eq. (1)]. The differences are significant, for example, there is almost a factor of 2 decrease between function values at radius 0.1 nm for 100 eV incident electrons when the tracking cut is lowered from 20 eV down to 7.4 eV. The difference is less pronounced (less than a factor of 2) at the same radius for 1 keV electrons. For both energies, the typical shift in position of the maximum is of the order of a few nanometers. These observations highlight the role of track-ends in the description of the energy deposition pattern at the nanoscale, while also underlining the necessity to always specify the value of tracking cut when proximity functions are calculated from MCTS codes.

B. Proton simulations

Figure 7 presents differential proximity functions obtained for 10^4 monoenergetic protons of 10 keV, 100 keV, and 1 MeV (larger statistics lead to prohibitive simulation durations). The results were
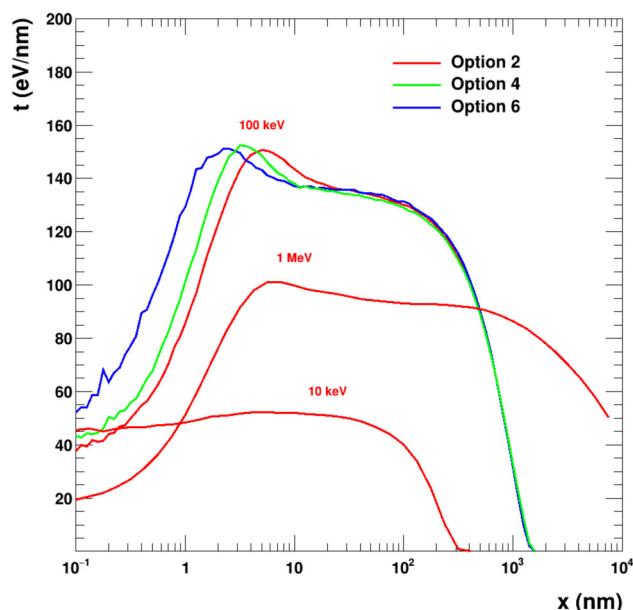
FIG. 7. (Differential) proximity functions $t(x)$ as a function of radius x for monoenergetic protons with incident energies of 10 keV, 100 keV, and 1 MeV. The "option 2" physics constructor has been used with its default tracking cut of 7.4 eV (red curves). The green and blue curves represent simulations at 100 keV using the "option 4" and "option 6" constructors, respectively.
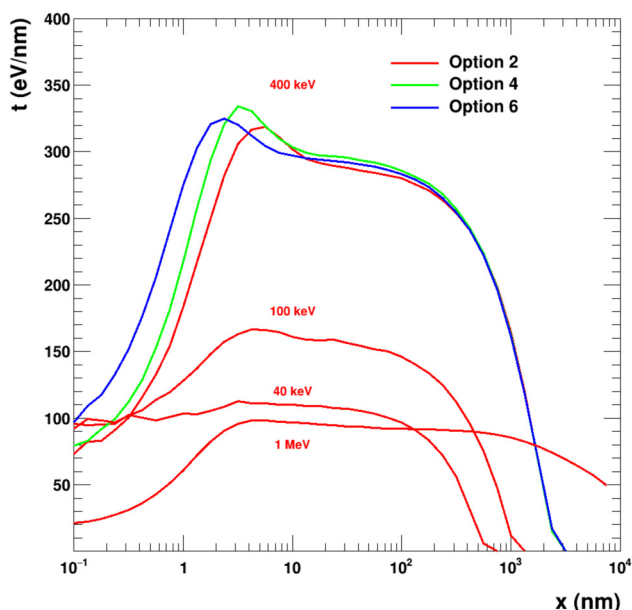
FIG. 8. (Differential) proximity functions $t(x)$ as a function of radius x for monoenergetic alpha particles with incident energies of 40 keV, 100 keV, 400 keV, and 1 MeV. The "option 2" physics constructor has been used with its default tracking cut of 7.4 eV (red curves). The green and blue curves represent simulations at 400 keV using the "option 4" and "option 6" constructors, respectively.

obtained using the Geant4-DNA "option 2" (default option) because it has the largest energy coverage for electrons (7.4 eV–1 MeV). The functions are represented up to 10^4 nm and show significantly larger values than for incident electrons. For example, at 100 keV, the maximum of the function for electrons reaches 22.4 eV/nm at 2.5 nm, while it reaches 151 eV/nm for protons at 5 nm. For this incident energy, where the proximity function is largest, we also show in this figure the results obtained with the "option 4" and "option 6" constructors. Profiles are similar, but sizeable differences persist at small distances (<10 nm). While the maxima are very close, the maximum for "option 6" is reached at shorter radius than for "option 4," and similarly "option 4" maximum is reached at shorter radius than "option 2." For example, the maximum for "option 6" is equal to 151 eV/nm and is reached at 2.2 nm, the maximum for "option 4" is equal to 153 eV/nm at 3.2 nm and the maximum for "option 2" is 151 eV/nm at 5 nm. This is again a consequence of inelastic cross sections being larger for "option 6" than "option 4" or "option 2," leading to larger energy deposition at smaller distances.

C. Alpha particles simulations

Figure 8 presents differential proximity functions obtained for 10^4 monoenergetic alpha particles of 40 keV, 100 keV, 400 keV, and 1 MeV. Note that the 40 keV and 400 keV alpha particles have similar speeds with protons of kinetic energy 10 keV and 100 keV shown in Fig. 7. The results were obtained using the Geant4-DNA

"option 2" (default option). The functions are represented up to 10^4 nm and show significantly larger values than for incident protons. For example, at 100 keV, the maximum reaches 167 eV/nm at about 4 nm (compared to 150 eV/nm at 5 nm for protons), and at 400 keV, the maximum of the function reaches 318 eV/nm at 5.6 nm. Similarly, as for protons, we have also added to this figure results obtained with the "option 4" and "option 6" constructors for 400 keV alpha particles. The profiles are similar, with values larger than for the proton case with the same physics constructors. For the same reason as for the proton case, the maximum value for "option 6" (303 eV/nm, located at 2.4 nm) occurs at a smaller radius than for "option 4" (334 eV/nm, 3.2 nm) and "option 2" (319 eV/nm, 5.6 nm).

D. Biophysical implications

Besides modern approaches to model the relative biological effectiveness (RBE),[61] many theoretical predictions of RBE are still based on microdosimetric concepts, such as the dose-weighted lineal energy in micro- or nano-meter size targets[62,63] or various clustering analysis of ionisations[64,65] or energy deposition[66] at the nanoscale. Proximity functions can be used to calculate the RBE in the context of the TDRA.[47] In this theory, the RBE is expressed as

$$\mathrm{RBE} = \frac{\zeta_{\mathrm{test}}}{\zeta_{\mathrm{ref}}}, \tag{4}$$

where the subscript "test" and "ref" denote the radiation under test and the reference radiation, respectively, and

$$\zeta = \int_0^\infty t(x)\gamma(x)dx, \qquad (5)$$

with $\gamma(x)$ being a biological function related to the interaction probability of sublesions (separated by a distance x) to form a lesion. In the special case, whereby the sublesion interaction probability is independent of distance (the so-called "site model" of the TDRA), the function $\gamma(x)$ is simply the geometrical proximity function of the target. In this special case ("site model"), Eq. (4) reduces to the ratio of y_D of Eq. (3). In the general case (or "distance model" of the TDRA), the form of $\gamma(x)$ depends on both the geometrical and biological properties of the system. A commonly used form for $\gamma(x)$ is that derived for V79 cells, which exhibits a rather constant value (±10%) up to about 10 nm, sharply falling (but not vanishing) at larger distances. Thus, as an application example of the present results, we can approximate $\gamma(x)$ by a step function, i.e., $\gamma(x) = 1$ for $x \leq 10$ nm and $\gamma(x) = 0$ for $x > 10$ nm. Inserting this approximate $\gamma(x)$ in Eq. (5) and using the track structure proximity results of this work to determine the function $t(x)$ entering Eq. (5), we can then use Eq. (4) to make a rough estimate of the variation of RBE with electron energy. The results for the
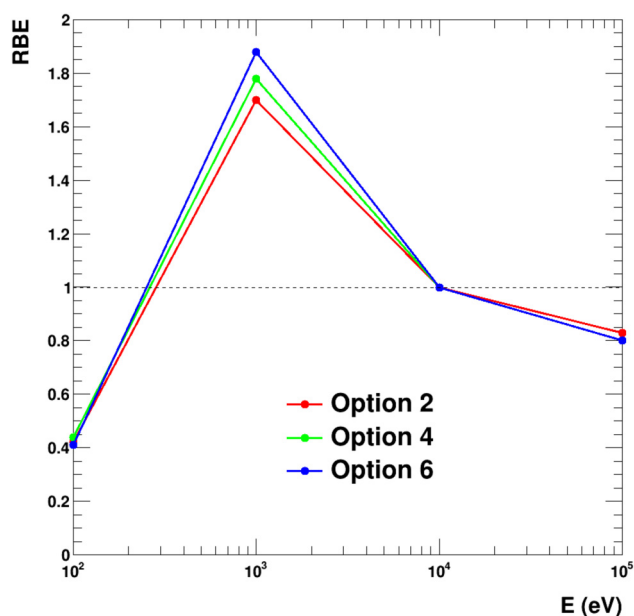
FIG. 9. RBE calculations as a function of incident kinetic energy for monoenergetic electrons with incident energies of 100 eV, 1 keV, 10 keV, and 100 keV. The "option 2" physics constructor has been used with its default tracking cut of 7.4 eV (red curves). The red, green, and blue curves show results obtained with the "option 2," "option 4," and "option 6" physics constructors, respectively. 10 keV is used as the "reference" radiation energy for the calculation of RBE (see Sec. III D for details).

different Geant4-DNA physics models ("option 2," "option 4," "option 6") are shown in Fig. 9. Since "option 4" has an upper energy limit of 10 keV (whereas "option 2" extends up to 1 MeV and "option 6" up to 256 keV), we have used this electron energy as the "reference" radiation in Eq. (4). Note also that the highest energy is at 100 keV since calculation times for higher energies become prohibitively long. It can be seen that the different physics models predict RBE values in good agreement (maximum discrepancy is equal to or less than about 10%). The results of Fig. 9 confirm the different radiobiological effectiveness (up to a factor of 2 in the present study) of electrons in the low-medium energy range as reviewed, for example, in Ref. 67. They also support the results of other microdosimetric studies that report RBE values of ~1.5 for soft X-rays (e.g., mammography) versus orthovoltage X-rays, see Ref. 68 and references therein.

IV. CONCLUSION

This work presents the first implementation in Geant4-DNA of a user application dedicated to the simulation of differential proximity functions of radiation tracks in liquid water. We have simulated such functions for incident electrons, protons, and alpha particles over a wide energy range. Selecting the three recommended physics constructors of Geant4-DNA, we have shown that all constructors predict similar proximity functions in both shape and absolute value at distances beyond a few nanometers. The influence of sub-excitation processes (vibrational excitation and molecular attachment) has been found to be rather small. For comparison with published data, we underlined the important role of very low energy electrons (i.e., track-ends) and, as a corollary, the necessity to use similar tracking cuts, and possibly simulations in the same phase (e.g., liquid versus vapor water). The biophysical implications of our proximity function calculations were examined in the context of the Theory of Dual Radiation Action (TDRA) which yielded up to a factor of 2 variation of the electron RBE in the energy range from 100 eV to 100 keV. The present application is fully included in Geant4 and is thus available to users in the open source for their own simulations. With the continuous on-going improvement and development of Geant4-DNA physics models for track structure simulations,[20] it is envisioned that the present application will be useful to extract differential proximity functions for a variety of radiation qualities in liquid water and other biological materials.

References

[1]M. Dingfelder, I. G. Jorjishvili, J. A. Gersh, and L. H. Toburen, Radiat. Prot. Dosimetry. **122**, 26 (2006).
[2]I. El Naqa, P. Pater, and J. Seuntjens, Phys. Med. Biol. **57**, R75 (2012).

[3]H. Nikjoo, D. Emfietzoglou, T. Liamsuwan, R. Taleei, D. Liljequist, and S. Uehara, Rep. Prog. Phys. **79**, 116601 (2016).

[4]W. Friedland, E. Schmitt, P. Kundrát, M. Dingfelder, G. Baiocco, S. Barbieri, and A. Ottolenghi, Sci. Rep. **7**, 45161 (2017).

[5]S. Incerti, A. Ivanchenko, M. Karamitros, A. Mantero, P. Moretto, H. N. Tran, B. Mascialino, C. Champion, V. N. Ivanchenko, M. A. Bernal, Z. Francis, C. Villagrasa, G. Baldacchino, P. Guèye, R. Capra, P. Nieminen, and C. Zacharatou, Med. Phy. **37**, 4692 (2010).

[6]P. Andreo, Phys. Med. Biol. **36**, 861 (1991).

[7]D. W. O. Rogers, Physi. Med. Biol. **51**, R287 (2006).

[8]I. Kyriakou, D. Emfietzoglou, V. Ivanchenko, M. C. Bordage, S. Guatelli, P. Lazarakis, H. N. Tran, and S. Incerti, J. Appl. Phys. **122**, 024303 (2017).

[9]P. Lazarakis, S. Incerti, V. Ivanchenko, I. Kyriakou, D. Emfietzoglou, S. Corde, A. B. Rosenfeld, M. Lerch, M. Tehei, and S. Guatelli, Biomed. Phys. Eng. Express **4**, 024001 (2018).

[10]J. M. Fernández-Varea, Radiat. Phys. Chem. **53**, 235 (1998).

[11]K. Wiklund, J. M. Fernández-Varea, and B. K. Lind, Phy. Med. Biol. **56**, 1985 (2011).

[12]M. Dingfelder, Health Phys. **103**, 590 (2012).

[13]G. Bäckström, M. E. Galassi, N. Tilly, A. Ahnesjö, and J. M. Fernández-Varea, Med. Phys. **40**, 064101 (2013).

[14]V. A. Semenenko, J. E. Turner, and T. B. Borak, Radiat. Environ. Bioph. **42**, 213 (2003).

[15]W. Friedland, M. Dingfelder, P. Kundrát, and P. Jacob, Mutat. Res. **711**, 28 (2011).

[16]T. Liamsuwan, D. Emfietzoglou, S. Uehara, and H. Nikjoo, Int. J. Radiat. Biol. **88**, 899 (2012).

[17]H. Nikjoo, S. Uehara, D. Emfietzoglou, and F. A. Cucinotta, Radiat. Meas. **41**, 1052 (2006).

[18]S. Incerti, G. Baldacchino, M. Bernal, R. Capra, C. Champion, Z. Francis, P. Guèye, A. Mantero, B. Mascialino, P. Moretto, P. Nieminen, C. Villagrasa, and C. Zacharatou, Int. J. Model. Simul. Sci. Comput. **01**, 157 (2010).

[19]M. A. Bernal, M. C. Bordage, J. M. C. Brown, M. Davídková, E. Delage, Z. El Bitar, S. A. Enger, Z. Francis, S. Guatelli, V. N. Ivanchenko, M. Karamitros, I. Kyriakou, L. Maigne, S. Meylan, K. Murakami, S. Okada, H. Payno, Y. Perrot, I. Petrovic, Q. T. Pham, A. Ristic-Fira, T. Sasaki, V. Štěpán, H. N. Tran, C. Villagrasa, and S. Incerti, Phys. Med. **31**, 861 (2015).

[20]S. Incerti, I. Kyriakou, M. A. Bernal, M. C. Bordage, Z. Francis, S. Guatelli, V. Ivanchenko, M. Karamitros, N. Lampe, S. B. Lee, S. Meylan, C. H. Min, W. G. Shin, P. Nieminen, D. Sakata, N. Tang, C. Villagrasa, H. N. Tran, and J. M. C. Brown, Med. Phys. **45**, e722 (2018).

[21]S. Agostinelli, J. Allison, K. Amako, J. Apostolakis, H. Araujo, P. Arce, M. Asai, D. Axen, S. Banerjee, G. Barrand, F. Behner, L. Bellagamba, J. Boudreau, L. Broglia, A. Brunengo, H. Burkhardt, S. Chauvie, J. Chuma, R. Chytracek, G. Cooperman, G. Cosmo, P. Degtyarenko, A. Dell'Acqua, G. Depaola, D. Dietrich, R. Enami, A. Feliciello, C. Ferguson, H. Fesefeldt, G. Folger, F. Foppiano, A. Forti, S. Garelli, S. Giani, R. Giannitrapani, D. Gibin, J. J. Gómez Cadenas, I. González, G. Gracia Abril, G. Greeniaus, W. Greiner, V. Grichine, A. Grossheim, S. Guatelli, P. Gumplinger, R. Hamatsu, K. Hashimoto, H. Hasui, A. Heikkinen, A. Howard, V. Ivanchenko, A. Johnson, F. W. Jones, J. Kallenbach, N. Kanaya, M. Kawabata, Y. Kawabata, M. Kawaguti, S. Kelner, P. Kent, A. Kimura, T. Kodama, R. Kokoulin, M. Kossov, H. Kurashige, E. Lamanna, T. Lampén, V. Lara, V. Lefebure, F. Lei, M. Liendl, W. Lockman, F. Longo, S. Magni, M. Maire, E. Medernach, K. Minamimoto, P. Mora de Freitas, Y. Morita, K. Murakami, M. Nagamatu, R. Nartallo, P. Nieminen, T. Nishimura, K. Ohtsubo, M. Okamura, S. O'Neale, Y. Oohata, K. Paech, J. Perl, A. Pfeiffer, M. G. Pia, F. Ranjard, A. Rybin, S. Sadilov, E. Di Salvo, G. Santin, T. Sasaki, N. Savvas, and Y. Sawada, Nucl. Instrum. Methods Phys. Res. Sect. A. **506**, 250 (2003).

[22]J. Allison, K. Amako, J. Apostolakis, H. Araujo, P. A. Dubois, M. Asai, G. Barrand, R. Capra, S. Chauvie, R. Chytracek, G. A. P. Cirrone, G. Cooperman, G. Cosmo, G. Cuttone, G. G. Daquino, M. Donszelmann, M. Dressel, G. Folger, F. Foppiano, J. Generowicz, V. Grichine, S. Guatelli, P. Gumplinger, A. Heikkinen, I. Hrivnacova, A. Howard, S. Incerti, V. Ivanchenko, T. Johnson, F. Jones, T. Koi, R. Kokoulin, M. Kossov, H. Kurashige, V. Lara, S. Larsson, F. Lei, O. Link, F. Longo, M. Maire, A. Mantero, B. Mascialino, I. McLaren, P. M. Lorenzo, K. Minamimoto, K. Murakami, P. Nieminen, L. Pandola, S. Parlati, L. Peralta, J. Perl, A. Pfeiffer, M. G. Pia, A. Ribon, P. Rodrigues, G. Russo, S. Sadilov, G. Santin, T. Sasaki, D. Smith, N. Starkov, S. Tanaka, E. Tcherniaev, B. Tome, A. Trindade, P. Truscott, L. Urban, M. Verderi, A. Walkden, J. P. Wellisch, D. C. Williams, D. Wright, and H. Yoshida, Nucl. Sci. IEEE Trans. **53**, 270 (2006).

[23]J. Allison, K. Amako, J. Apostolakis, P. Arce, M. Asai, T. Aso, E. Bagli, A. Bagulya, S. Banerjee, G. Barrand, B. R. Beck, A. G. Bogdanov, D. Brandt, J. M. C. Brown, H. Burkhardt, P. Canal, D. Cano-Ott, S. Chauvie, K. Cho, G. A. P. Cirrone, G. Cooperman, M. A. Cortés-Giraldo, G. Cosmo, G. Cuttone, G. Depaola, L. Desorgher, X. Dong, A. Dotti, V. D. Elvira, G. Folger, Z. Francis, A. Galoyan, L. Garnier, M. Gayer, K. L. Genser, V. M. Grichine, S. Guatelli, P. Guèye, P. Gumplinger, A. S. Howard, I. Hřivnáčová, S. Hwang, S. Incerti, A. Ivanchenko, V. N. Ivanchenko, F. W. Jones, S. Y. Jun, P. Kaitaniemi, N. Karakatsanis, M. Karamitros, M. Kelsey, A. Kimura, T. Koi, H. Kurashige, A. Lechner, S. B. Lee, F. Longo, M. Maire, D. Mancusi, A. Mantero, E. Mendoza, B. Morgan, K. Murakami, T. Nikitina, L. Pandola, P. Paprocki, J. Perl, I. Petrović, M. G. Pia, W. Pokorski, J. M. Quesada, M. Raine, M. A. Reis, A. Ribon, A. Ristić Fira, F. Romano, G. Russo, G. Santin, T. Sasaki, D. Sawkey, J. I. Shin, I. I. Strakovsky, A. Taborda, S. Tanaka, B. Tomé, T. Toshito, H. N. Tran, P. R. Truscott, L. Urban, V. Uzhinsky, J. M. Verbeke, M. Verderi, B. L. Wendt, H. Wenzel, D. H. Wright, D. M. Wright, T. Yamashita, J. Yarba, and H. Yoshida, Nucl. Instrum. Methods Phys. Res. Sect. A. **835**, 186 (2016).

[24]M. Terrissol, Thesis (Toulouse University, 1978).

[25]I. Plante and F. A. Cucinotta, Radiat. Prot. Dosim. **166**, 19 (2015).

[26]M. U. Bug, W. Yong Baek, H. Rabus, C. Villagrasa, S. Meylan, and A. B. Rosenfeld, Radiat. Phys. Chem. **130**, 459 (2017).

[27]W. Friedland, P. Kundrát, E. Schmitt, J. Becker, and W. Li, "Modeling DNA damage by photons and light ions over energy ranges used in medical applications," Radiat. Prot. Dosimetry (published online).

[28]H. Nikjoo, R. Taleei, T. Liamsuwan, D. Liljequist, and D. Emfietzoglou, Radiat. Phys. Chem. **128**, 3 (2016).

[29]J. M. Fernández-Varea, X. Llovet, and F. Salvat, Surf. Interface Anal. **37**, 824 (2005).

[30]D. Emfietzoglou and H. Nikjoo, Radiat. Res. **163**, 98 (2005).

[31]F. Salvat and J. M. Fernández-Varea, Metrologia **46**, S112 (2009).

[32]D. Emfietzoglou, I. Kyriakou, R. Garcia-Molina, I. Abril, and H. Nikjoo, Radiat. Res. **180**, 499 (2013).

[33]M. Dingfelder, Appl. Radiat. Isotopes **83**(Part B), 142 (2014).

[34]D. Emfietzoglou, I. Kyriakou, R. Garcia-Molina, and I. Abril, Surf. Interface Anal. **49**, 4 (2017).

[35]R. Garcia-Molina, I. Abril, I. Kyriakou, and D. Emfietzoglou, Surf. Interface Anal. **49**, 11 (2016).

[36]N. Lampe, M. Karamitros, V. Breton, J. M. C. Brown, D. Sakata, D. Sarramia, and S. Incerti, Phys. Med. **48**, 146 (2018).

[37]H. Nikjoo, P. O'Neill, W. E. Wilson, and D. T. Goodhead, Radiat. Res. **156**, 577 (2001).

[38]H. H. Rossi and M. Zaider, *Microdosimetry and its Applications* (Springer, 1996).

[39]*International Commission on Radiation Units and Measurements* (ICRU, Bethesda, MD, 1983), see https://icru.org/reports/reports/microsimetry-report-36.

[40]H. Nikjoo, S. Uehara, D. Emfietzoglou, and L. Pinsky, Radiat. Prot. Dosim. **143**, 145 (2011).

[41]E. L. Alpen, *Radiation Biophysics* (Academic Press, 1997).

[42]A. M. Kellerer and H. H. Rossi, Radiat. Res. **75**, 471 (1978).

[43]D. Chmelevsky, A. M. Kellerer, M. Terrissol, and J. P. Patau, Radiat. Res. **84**, 219 (1980).

[44]D. J. Brenner and M. Zaider, Radiat. Res. **98**, 14 (1984).

[45]G. Leuthold and G. Burger, Radiat. Environ. Bioph. **27**, 177 (1988).

[46]Dayashankar and M. A. Prasad, Radiat. Res. **121**, 142 (1990).

[47]R. Taschereau, R. Roy, and J. Pouliot, Med. Dosim. **28**, 21 (2003).

[48]J. Chen and A. M. Kellerer, Radiat. Prot. Dosimetry **122**, 56 (2006).

[49]M. Zaider, D. J. Brenner, and W. E. Wilson, Radiat. Res. **95**, 231 (1983).

[50]D. Dabli, Thesis (Clermont-Ferrand 2 University, 2010).

[51]D. Emfietzoglou, G. Papamichael, and H. Nikjoo, Radiat. Res. **188**, 355 (2017).

[52]D. Emfietzoglou, F. A. Cucinotta, and H. Nikjoo, Radiat. Res. **164**, 202 (2005).

[53]D. Emfietzoglou, Radiat. Phys. Chem. **66**, 373 (2003).

[54]I. Kyriakou, S. Incerti, and Z. Francis, Med. Phys. **42**, 3870 (2015).

[55]I. Kyriakou, M. Šefl, V. Nourry, and S. Incerti, J. Appl. Phys. **119**, 194902 (2016).

[56]M. C. Bordage, J. Bordes, S. Edel, M. Terrissol, X. Franceries, M. Bardiès, N. Lampe, and S. Incerti, Phys. Medica. **32**, 1833 (2016).

[57]S. Incerti, B. Suerfu, J. Xu, V. Ivantchenko, A. Mantero, J. M. C. Brown, M. A. Bernal, Z. Francis, M. Karamitros, and H. N. Tran, Nucl. Instrum. Methods Phys. Res. Sect. B. **372**, 91 (2016).

[58]R. Brun and F. Rademakers, Nuc. Instrum. Methods Phys. Res. Sect. A. **389**, 81 (1997).

[59]C. S. Wuu and M. Zaider, Med. Phys. **25**, 2186 (1998).

[60]M. Karamitros, S. Luan, M. A. Bernal, J. Allison, G. Baldacchino, M. Davidkova, Z. Francis, W. Friedland, V. Ivantchenko, A. Ivantchenko, A. Mantero, P. Nieminem, G. Santin, H. N. Tran, V. Stepan, and S. Incerti, J. Comput. Phys. **274**, 841 (2014).

[61]L. Bodgi, A. Canet, L. Pujo-Menjouet, A. Lesne, J.-M. Victor, and N. Foray, J. Theor. Biol. **394**, 93 (2016).

[62]L. Lindborg, M. Hultqvist, TÅ Carlsson, and H. Nikjoo, Phys. Med. Biol. **58**, 3089 (2013).

[63]C. S. Wuu, P. Kliauga, and H. I. Amols, Int. J. Radiat. Oncol. **36**, 689 (1996).

[64]V. Michalik, Phys. Med. Biol. **36**, 1001 (1991).

[65]F. Verhaegen and B. Reniers, Radiat. Res. **162**, 592 (2004).

[66]F. Villegas, G. Bäckström, N. Tilly, and A. Ahnesjö, Med. Phys. **43**, 6322 (2016).

[67]H. Nikjoo and L. Lindborg, Phys. Med. Biol. **55**, R65 (2010).

[68]A. M. Kellerer, Radiat. Res. **158**, 13 (2002).

[69]S. Uehara, H. Nikjoo, and D. T. Goodhead, Phys. Med. Biol. **38**, 1841 (1993).